Journal of Power Sources 189 (2009) 503–506

Contents lists available at ScienceDirect

Journal of Power Sources

journal homepage: www.elsevier.com/locate/jpowsour

Short communication

# Electrochemical intercalation of lithium ions into $LiV_3O_8$ in an aqueous electrolyte

G.J. Wang[a,c], Q.T. Qu[a], B. Wang[a], Y. Shi[a], S. Tian[a], Y.P. Wu[a,b,*], R. Holze[b]

[a] New Energy and Materials Laboratory (NEML), Department of Chemistry & Shanghai Key Laboratory of Molecular Catalysis and Innovative Materials, Fudan University, Shanghai 200433,China
[b] Institut für Chemie, AG Elektrochemie, Technische Universität Chemnitz, D-09111 Chemnitz, Germany
[c] Department of Chemistry and Materials Science, Nanjing Forestry University, Nanjing 210037, China

ARTICLE INFO

*Article history:*
Received 13 August 2008
Received in revised form 1 November 2008
Accepted 3 November 2008
Available online 8 November 2008

*Keywords:*
Aqueous rechargeable lithium battery (ARLB)
Cyclic voltammogram
$LiV_3O_8$
Aqueous electrolyte

ABSTRACT

Electrochemical intercalation of lithium ions from a saturated $LiNO_3$ aqueous electrolyte solution into $LiV_3O_8$ prepared by a solid-state reaction at 680 °C was studied with cyclic voltammetry and electrochemical impedance spectroscopy (EIS). Results show that there are three steps of intercalation in the presence of an aqueous electrolyte, in agreement with those previously observed with organic liquid electrolytes. In addition, variations of several parameters including the charge transfer resistance ($R_{ct}$), the capacitance of the double layer ($C_{DL}$), the Warburg diffusion impedance ($Z_w$), and diffusion coefficient of lithium ions ($D_{Li^+}$) during the intercalation process are reported.



## 1. Introduction

Lithium vanadium oxide, $Li_{1+x}V_3O_8$, has been studied as a promising cathode material in rechargeable lithium batteries for over 50 years because of its low cost, high electronic conductivity, potentially high reversible capacity and good cycling behavior after the first proposal by Wadsley [1–7]. This oxide has a layered structure where pre-existing $Li^+$ ions at octahedral sites attach adjacent layers strongly leading to outstanding cycling stability. Over three equivalents of $Li^+$ ions can be intercalated/extracted in $LiV_3O_8$ reversibly resulting in larger practical discharge capacities as compared with other transition metals such as $LiCoO_2$, $LiMn_2O_4$. The traditional synthesis method is the solid-state reaction between $Li_2CO_3$ and $V_2O_5$ at 680 °C [7,8]. In order to improve the electrochemical performance of $Li_{1+x}V_3O_8$, much effort has been made such as adaptation of the samples with different degrees of crystallinity [5,9–12], introduction of alien atoms and molecules between the layers [9,13–15], and the electrochemical profiles of $Li_{1+x}V_3O_8$ in organic electrolyte solutions have been extensively investigated [16–23]. Furthermore, $Li/LiV_3O_8$ battery system having relatively high energy density and high voltage was constructed and studied for practical use [24].

However, in current commercial lithium batteries, the flammable organic liquid electrolytes are being used. Their safety and reliability are serious problems in recent years even in the case of lithium ion batteries with small capacity. In the case of large-scale power energy storage such as load-levelling in the electric grid or storage of solar and wind energy, safety and reliability will be even more challenging though so far there is no report about their applications in these areas. As a result, lead-acid rechargeable batteries are widely used for these purposes due to their good safety and low cost although they cause serious environmental pollution. It is urgent to find new and cheap systems to substitute lead-acid rechargeable batteries.

Recently, an aqueous rechargeable batteries (ARLB) using lithium vanadium oxide ($LiV_3O_8$) as the anode, other transition metal oxides such as $LiNi_{0.81}Co_{0.19}O_2$, $LiCoO_2$, $LiMn_2O_4$ and $LiNi_{1/3}Co_{1/3}Mn_{1/3}O_2$ [25–28] as the cathode and aqueous solutions of lithium salts as the electrolyte was reported. It is evident that the electrochemical lithium intercalation reaction in aqueous electrolytes can be made possible by selecting appropriate transition metal oxides and electrolytes. Initial results show that the ARLBs have the following advantages: (a) high ion conductivity compared to the nonaqueous lithium ion cells, (b) promising high rate capability, (c) relatively high energy and power densities which are

* Corresponding author at: Cochairman of IUPAC International Symposium on Novel Materials and Their Synthesis (NMS), Department of Chemistry, Fudan University, Shanghai 200433, China. Tel.: +86 21 5566 4223; fax: +86 21 5566 4223.
*E-mail addresses:* wuyp@fudan.edu.cn (Y.P. Wu), rudolf.holze@chemie.tu-chemnitz.de (R. Holze).

0378-7753/$ – see front matter © 2008 Elsevier B.V. All rights reserved.
doi:10.1016/j.jpowsour.2008.11.006

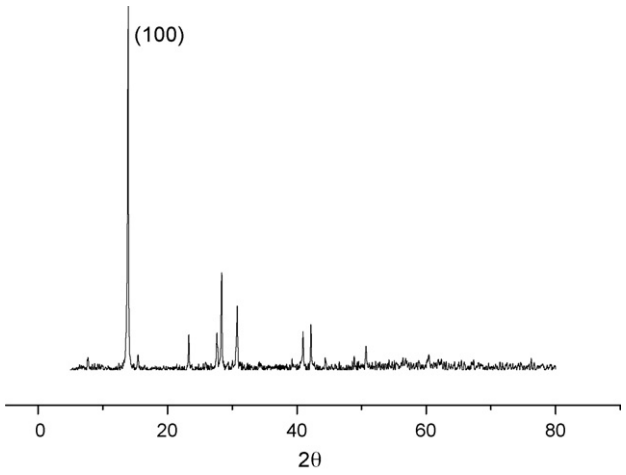


**Fig. 1.** XRD pattern for the as-prepared $LiV_3O_8$.

competitive with those of lead-acid or Ni–Cd cells, (d) inherent safety, (e) no environmental pollution, (f) no safety problem even in the case of misuse, and (g) low cost.

However, early ARLBs show a rapid capacity loss with cycling [29]. In order to understand the reasons for the capacity decay or fading, the electrochemical performance of the electrode materials in aqueous electrolytes should be well understood. In organic electrolyte, lithium intercalation behaviors of $Li_{1+x}V_3O_8$ were reported [16–18,30–32]. These results indicates that lithium intercalation to $Li_{1+x}V_3O_8$ proceeds as a single-phase reaction for $0 < x < 1.5{\sim}2.0$, followed by a two-phase reaction for $1.5{\sim}2.0 < x < 3.2$, and a single-phase reaction for $3.2 < x < 4.0$. In this paper, we investigated the electrochemical behavior of lithium ion intercalation into pristine $LiV_3O_8$ in aqueous electrolytes to provide better understanding for ARLB systems.

## 2. Experimental

$LiV_3O_8$ was prepared by heating a mixture of $Li_2CO_3$ and $V_2O_5$ after milling in the molar ratio of 1:3 at 680 °C for 24 h [26]. Its crystal structure was characterized by X-ray powder diffraction (XRD) using the Bruker Analytical X-ray Systems with Cu Kα radiation source filtered by a Ni thin plate. The morphology was observed with a scanning electron microscope (SEM, Philips XL 300).

A three-electrode electrochemical cell was employed for the measurement of cyclic voltammograms (CV) in saturated $LiNO_3$ aqueous electrolyte. Saturated calomel electrode (SCE) and Ni-mesh were used as the reference and the counter electrodes. The working electrode was prepared by pressing a powdered mixture of the sample, acetylene black and poly(tetrafluoroethylene) (PTFE) in a weight ratio of 80:10:10. Electrochemical impedance spectroscopy (EIS, EG and G5210) was carried out at room temperature using the above-described three-electrode electrochemical cell. The excitation voltage applied to the cell was 5 mV and the frequency range was 100 kHz to 10 mHz.

## 3. Results and discussion

XRD pattern of the prepared $LiV_3O_8$ is shown in Fig. 1. The strong peak at $2\theta = 13°$ is assigned to the diffraction of (1 0 0) planes indicating the layered structure of $LiV_3O_8$. These layers consist of octahedral $VO_6$ and trigonal bipyramid of $VO_5$ which share a corner with the octahedral. The scanning electron micrograph of the as-prepared $LiV_3O_8$ shows a layered morphology in Fig. 2. The particle size of $LiV_3O_8$ is in the range of 6–10 μm. These results suggest

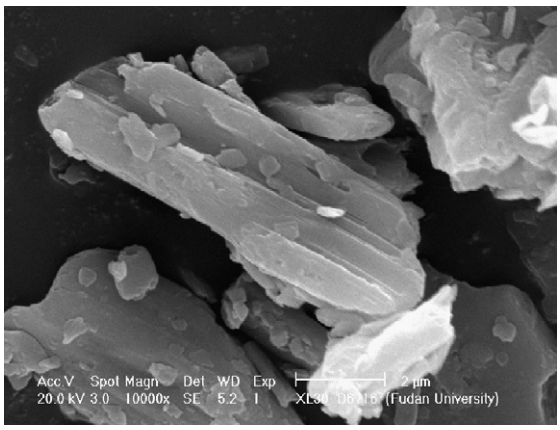


**Fig. 2.** Scanning electron micrograph of the as-prepared $LiV_3O_8$ particles.

that there is a preferred orientation and future investigation is needed.

The CV of $LiV_3O_8$ in saturated $LiNO_3$ aqueous electrolyte at a scan rate of 0.08 mV $s^{-1}$ during the second scan is shown in Fig. 3. It can be seen that there are three current peaks located at $E_{SCE} = -0.320$, $-0.355$ and $-0.490$ V which correspond to intercalation of lithium ions during the negative-going scan. The large current rise at $E_{SCE} = -0.9$ V is attributed to hydrogen evolution. In the meanwhile, there are three corresponding current peaks located $E_{SCE} = -0.089$, $-0.181$ and $-0.382$ V during the deintercalation process, respectively. According to the above results and the intercalation behavior of $LiV_3O_8$ in the organic electrolytes [16–18,23,30–33], it is suggested that the electrochemical behavior of lithium ion in $LiV_3O_8$ lattice in aqueous solution is similar to that in organic electrolyte and there are perhaps also three steps when lithium ions intercalate into $Li_{1+x}V_3O_8$ lattice in the aqueous electrolyte: (i) single-phase region for the range $0 < x < 2.0$ in $Li_{1+x}V_3O_8$; (ii) two-phase reaction for $2.0 < x < 3.2$, and (iii) single-phase reaction for $3.2 < x < 4.0$. Phase transformation occurs at $x = 2.0$ from the original $LiV_3O_8$ phase to the second $Li_4V_3O_8$ one. As to the detailed steps, further work is necessary.

The Nyquist plots for $LiV_3O_8$ at various potentials are shown in Fig. 4. All the Nyquist plots consist of two parts, i.e. an arc in the high frequency range and an inclining line in the low frequency range. The high frequency range generally corresponds to the charge transfer, and the inclining line in the low frequency range reflects the solid-state diffusion process of lithium ions in $LiV_3O_8$. According to the experimental results obtained in this work, an equivalent circuit, as shown in Fig. 5, is proposed to fit the

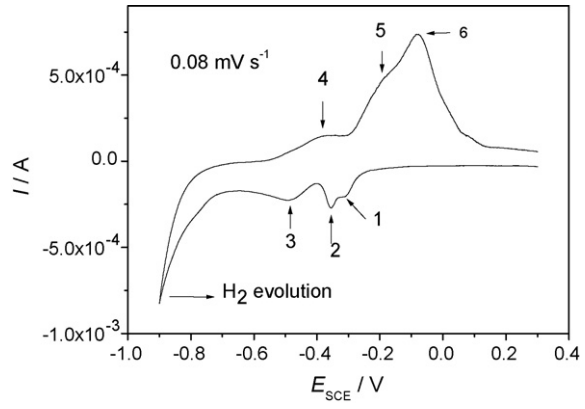


**Fig. 3.** Cyclic voltammogram of $LiV_3O_8$ in saturated $LiNO_3$ aqueous solution at a slow scan rate of 0.08 mV $s^{-1}$.

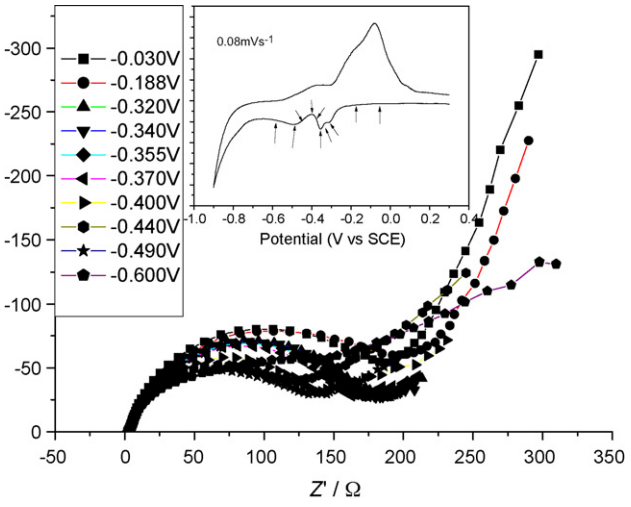


**Fig. 4.** EIS spectra of $LiV_3O_8$ at different potentials.

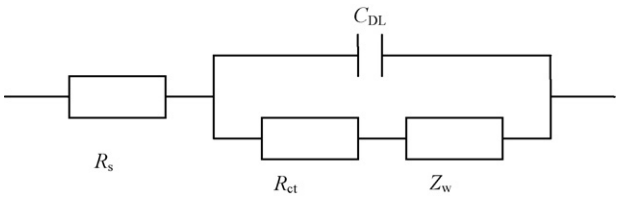


**Fig. 5.** Equivalent circuit of Nyquist plots in Fig. 4.

impedance spectra during the discharge process. In this equivalent circuit, $R_s$ represents the ohmic resistance of the aqueous solution, $R_{ct}$ is the charge transfer resistance, and the capacitance of the double layer and the Warburg impedance are represented by $C_{DL}$ and $Z_w$, respectively. The values of the parameters calculated from the impedance data during the discharge process are summarized in Table 1.

The parameters of the equivalent circuit from fitting the experimental impedance data of the $LiV_3O_8$ electrode with the decrease of the potential are shown in Fig. 6. It can be seen from Fig. 6a that $R_s = 3.177\ \Omega$ stays constant with decreasing potential. Apparently the electrolyte resistance does not change during the discharge process. From Fig. 6a and b it can be seen that $R_{ct}$ and $Z_w$ present the same trend in change. When the potential shifts into the negative direction, $R_{ct}$ and $Z_w$ increase gradually. When lithium ions intercalate into tetrahedral sites of the $LiV_3O_8$, they increase and then decrease subsequently. When lithium ions enter into octahedral sites of $LiV_3O_8$, they increase and then decrease again obviously. Fig. 6c shows $C_{DL} = 0.51$ mF at the beginning, and then increases with the negative shift of the potential. The $C_{DL}$ decreases

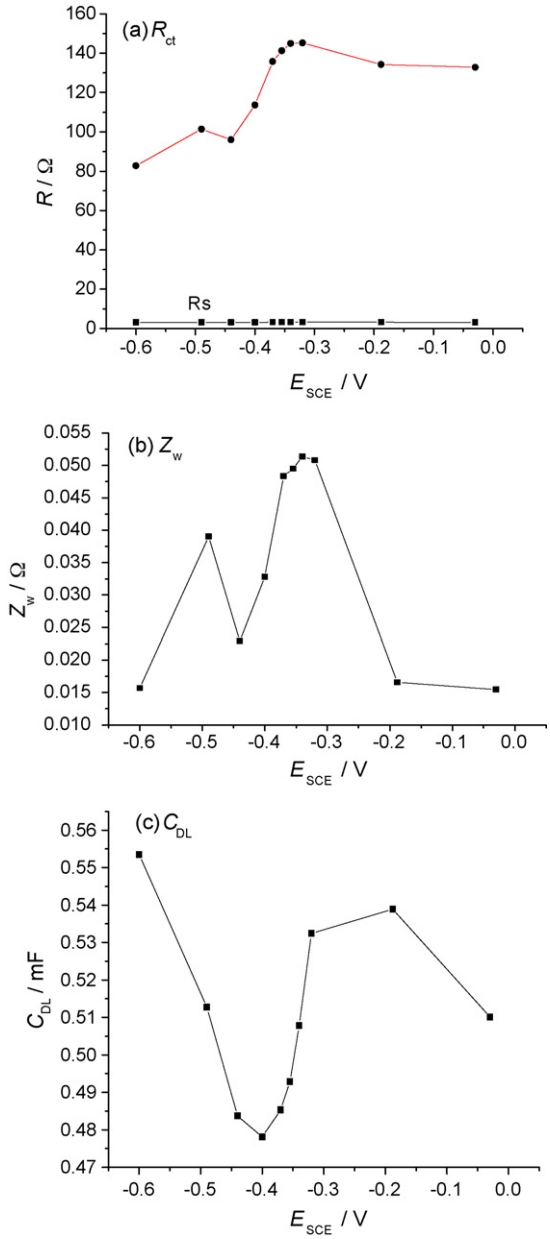


**Fig. 6.** Variations of component parameters in equivalent circuit of Fig. 5 with the potential.

gradually during the intercalation of lithium ions into tetrahedral sites of $LiV_3O_8$ and then reaches to the minimum of 0.4781 mF at $E_{SCE} = -0.400$ V. Subsequently, the value of $C_{DL}$ increases gradually up to the maximum.

**Table 1**
Data from fits of the impedance spectra of the $LiV_3O_8$ electrode during the lithium intercalation process.

| Potential (V) | $R_s$ (Ω) | $C_{DL}$ (mF) | $R_{ct}$ (Ω) | $Z_w$ (Ω) | $D_{Li^+}$ ($\times 10^{-9}$ cm$^2$ s$^{-1}$) |
|---|---|---|---|---|---|
| −0.030 | 3.106 | 0.5101 | 132.8 | 0.01548 | 4.479 |
| −0.188 | 3.199 | 0.5389 | 134.2 | 0.0166 | 7.340 |
| −0.320 | 3.234 | 0.5324 | 145.2 | 0.05083 | 10.02 |
| −0.340 | 3.226 | 0.5078 | 144.9 | 0.05136 | 4.395 |
| −0.355 | 3.205 | 0.4929 | 141.2 | 0.04949 | 5.179 |
| −0.370 | 3.19 | 0.4853 | 135.7 | 0.04836 | 10.67 |
| −0.400 | 3.169 | 0.4781 | 113.6 | 0.03281 | 9.041 |
| −0.440 | 3.149 | 0.4837 | 95.98 | 0.02291 | 6.260 |
| −0.490 | 3.154 | 0.5127 | 101.3 | 0.03903 | 11.426 |
| −0.600 | 3.136 | 0.5535 | 82.7 | 0.01571 | 5.447 |

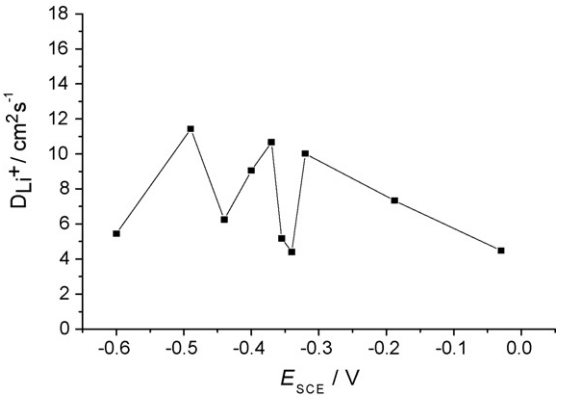


**Fig. 7.** Variations of diffusion coefficient of lithium ion at different polarization potentials during the lithium ion intercalation.

The diffusion coefficient of lithium ion can be calculated from the plots in the low frequency region according to the following equation [34]:

$$D_{Li^+} = \frac{R^2T^2}{2A^2n^4F^4C^2\sigma^2} \quad (1)$$

where $R$ is gas constant, $T$ is absolute temperature, $n$ is the number of electron(s) per molecule, $A$ is surface area, $F$ is Faraday constant, $C$ is concentration, $D_{Li^+}$ is diffusion coefficient, and $\sigma$ is the Warburg factor which is related to $Z_{re}$:

$$Z_{re} = R_D + R_L + \sigma\omega^{-1/2} \quad (2)$$

where $Z_{re}$, $R_D$ and $R_L$ are the real part of the resistance, bulk resistance of the solution and the resistance corresponding to the charge transfer, respectively. The diffusion coefficients of lithium ion at different potentials are also listed in Table 1. The variation of $D_{Li^+}$ with the potential during the lithium ion intercalation process is shown in Fig. 7. It can be seen that the diffusion coefficient of lithium ion gradually increases at the beginning of the intercalation process. When the potential is shifted to $E_{SCE} = -0.320$ V, i.e. lithium ions entering into the first tetrahedral sites of the $LiV_3O_8$, $D_{Li^+}$ arrives at the first maximum. Subsequently, the $D_{Li^+}$ decreases gradually and then increases again during lithium ions enter into the second tetrahedra sites of the $LiV_3O_8$. In succession, $D_{Li^+}$ decreases again and then increases suddenly when lithium ions intercalate into octahedra sites of $LiV_3O_8$. When the potential is shifted to $E_{SCE} = -0.600$ V, $D_{Li^+}$ decreases again.

Evidently, the main reason for these changes for $R_{ct}$, $Z_w$, $C_{DL}$ and $D_{Li^+}$ is related to structure or phase changes after lithium intercalation. Further studies are necessary for a deeper understanding of the associated mechanism.

## 4. Conclusion

Measurements of cyclic voltammetry and electrochemical impedance spectroscopy of $LiV_3O_8$ in saturated $LiNO_3$ aqueous solution show that the intercalation and deintercalation of lithium ions are similar to that in organic liquid electrolytes. There are also three steps of lithium ion intercalation reaction for $LiV_3O_8$ in the aqueous solution, locating at $E_{SCE} = -0.320$, $-0.355$ and $-0.490$ V, which agree well with those in the organic electrolytes. The parameters of lithium ions intercalation kinetics of $LiV_3O_8$ in the aqueous electrolyte including $R_s$, $R_{ct}$, $Z_w$, $C_{DL}$ and $D_{Li^+}$ vary with potential. These first results provide some clues for further research on safe and reliable aqueous recharge lithium batteries (ARLBs).

## Acknowledgements

Financial support from National Basic Research Program of China (973 Program No.: 2007CB209702) and Alexander von Humboldt Foundation is gratefully appreciated.

## References

[1] A.D. Wadsley, Acta. Crystallogr. 10 (1957) 261.
[2] D.G. Wickham, J. Inorg. Nucl. Chem. 27 (1965) 1939.
[3] J.M. Tarascon, M. Armand, Nature 414 (2001) 359.
[4] G. Pistoia, S. Panero, M. Tocci, R.V. Moshtev, V. Manev, Solid State Ionics 13 (1984) 311.
[5] K. Nassau, D.W. Murphy, J. Non-Cryst. Solids 44 (1981) 297.
[6] X. Zhang, R. Frech, Electrochim. Acta 43 (1998) 861.
[7] J. Kawakita, Y. Katayama, T. Muria, T. Kishi, Solid State Ionics 107 (1998) 145.
[8] A.S. Yu, N. Kumagai, Z.L. Liu, J.Y. Lee, J. Power Sources 74 (1998) 117.
[9] M. Pasquali, G. Pistoia, M. Tocci, V. Manev, R.V. Moshtev, J. Electrochem. Soc. 133 (1986) 2454.
[10] G. Pistoia, M. Pasquali, G. Wang, L. Li, J. Electrochem. Soc. 137 (1990) 2365.
[11] K. West, B. Zachau-Christiansen, S. Skaarup, Y. Saidi, J. Barker, I.I. Olsen, R. Pynenburg, R. Koksbang, J. Electrochem. Soc. 143 (1996) 820.
[12] N. Kumagai, A. Yu, J. Electrochem. Soc. 144 (1997) 830.
[13] V. Manev, A. Momchilov, A. Nassalevska, G. Pistoia, M. Pasquali, J. Power Sources 54 (1995) 501.
[14] G. Pistoia, G. Wang, D. Zane, Solid State Ionics 76 (1995) 285.
[15] J. Kawakita, K. Makino, Y. Katayama, T. Miura, T. Kishi, Solid State Ionics 99 (1997) 165.
[16] J. Kawakita, T. Miura, T. Kishi, J. Power Sources 83 (1999) 79.
[17] J. Kawakita, T. Kato, Y. Katayama, T. Miura, T. Kishi, J. Power Sources 81/82 (1999) 448.
[18] J. Kawakita, T. Miura, T. Kishi, Solid State Ionics 120 (1999) 109.
[19] G.Q. Liu, C.L. Zeng, K. Yang, Electrochim. Acta 47 (2002) 3239.
[20] S. Jouanneau, A. Verbaere, S. Lascaud, D. Guyomard, Solid State Ionics 177 (2006) 311.
[21] T.J. Patey, S.H. Ng, R. Büchel, N. Tran, F. Krumeich, J. Wang, H.K. Liu, P. Novák, Electrochem, Solid State Lett. 11 (2008) A46.
[22] H. Liu, H. Yang, T. Huang, Mater. Sci. Eng. B: Solid 143 (2007) 60.
[23] O.A. Brylev, O.A. Shlyakhtin, A.V. Egorov, Y.D. Tretyakov, J. Power Sources 164 (2007) 868.
[24] K. Takei, N. Terada, T. Iwahori, T. Tanaka, H. Mishima, K. Takeuchi, J. Power Sources 68 (1997) 78.
[25] J. Köhler, H. Makihara, H. Uegaito, H. Inoue, M. Toki, Electrochim. Acta 46 (2000) 59.
[26] G.J. Wang, L.J. Fu, N.H. Zhao, L.C. Yang, Y.P. Wu, H.Q. Wu, Angew. Chem. Int. Ed. 46 (2007) 295.
[27] G.J. Wang, H.P. Zhang, L.J. Fu, B. Wang, Y.P. Wu, Electrochem. Commun. 9 (2007) 1873.
[28] G.J. Wang, L.J. Fu, B. Wang, N.H. Zhao, Y.P. Wu, R. Holze, J. Appl. Electrochem. 38 (2008) 579.
[29] W. Li, J.R. Dahn, D. Wainwright, Science 264 (1994) 1115.
[30] G. Pistoia, M. Pasquali, M. Tocci, R.V. Moshtev, V. Manev, J. Electrochem. Soc. 132 (1985) 281.
[31] A. Hammou, A. Hammouche, Electrochim. Acta 33 (1988) 1719.
[32] I.D. Raistrick, Rev. Chim. Miner. 21 (1984) 456.
[33] S. Jouanneau, A. Verbaere, D. Guyomard, J. Solid State Chem. 178 (2005) 22.
[34] A.J. Bard, L.R. Faulkner, Electrochemical Methods Fundamentals and Applications, John Weily & Sons, Inc., 1980, p. 328.